Formulation of Reduced-order Models for Blade-vortex Interactions Using Modified Volterra Kernels

Angela Wong[1], Fred Nitzsche[2] and Mahmood Khalid[3]

[1,2]*Department of Mechanical and Aerospace Engineering, Carleton University*
Ottawa, ON, K1S 5B6, Canada

[3]*Institute for Aerospace Research, National Research Council Canada*
Ottawa, ON, K1A 0R6, Canada

Email: *Fred_Nitzsche@carleton.ca*

Abstract

The theory of Volterra integral series for nonlinear systems is applied to the prediction of the aerodynamic response of an NACA 0012 airfoil experiencing blade-vortex interaction. The phenomenon is modeled in two-dimensions using Euler/Navier-Stokes description of the flow. The resulting unsteady lift time sequences are appropriately combined to form a training dataset to identify the Volterra kernels that characterize the reduced-order model based on the Volterra integral series. Next, the response predicted by the reduced-order model is compared to new data produced by the Euler/Navier-Stokes simulations to which the reduced-order model has never been exposed. The lift time histories predicted by the reduced-order model and the corresponding Euler/Navier-Stokes simulations are shown to be in respectable agreement.

Nomenclature

c	Airfoil chord
c_j, d_k	Volterra kernels basis functions expansion coefficients
C_L	Airfoil instantaneous lift coefficient
C_p	Airfoil instantaneous pressure coefficient
ΔC_L	Maximum lift coefficient during BVI
K_1, K_2, K_3	First, second and third-order Volterra kernels
t, t_1, t_2	Instants of time
u_∞	Flow undisturbed velocity
(x_0, y_0)	Initial position of vortex core from airfoil leading edge
(x, y)	Instantaneous position of vortex core from airfoil leading edge
$z(t)$	Volterra series output function
$\alpha(\tau)$	Volterra series input function
$z_1(t), z_2(t), z_3(t)$	First, second and third-order Volterra functionals (linear, bilinear and tri-linear outputs of Volterra series)
Γ	Vortex circulation
ζ_j, μ_k	Volterra kernels basis functions (first and second-order)
$\tau, \tau_1, \tau_2, \tau_3$	Dummy time variables
τ_j, τ_{jk}	Time constants of Volterra kernels basis functions (first and second order)

Introduction

With the increasing usage of modern rotorcraft, the focus of most blade-vortex interaction (BVI) research is on the effects of unsteady impulsive loading on the rotor blades and the associated noise generated during the process. It is already well understood that BVI is essentially three-dimensional and unsteady phenomenon, as the tip helical vortex filaments produced by previous blades passages intersect the on-coming blades at different angles. However there are two orientations of the interaction that are of particular concern. The first is the case when the vortex axis of rotation is perpendicular to the leading edge of the on-coming blade, as shown in Fig. 1a. The second is the case when the vortex axis of rotation is parallel to the leading edge of the blade, as shown in Fig. 1b. By comparing the two orientations in Fig. 1, the area affected by the parallel is greater then that affected by the perpendicular case. As the vortex travels parallel to the leading edge of the blade, a larger span of the blade will be simultaneously affected by the vortex. In fact, Martin *et al.* (Ref. 1) identified in wind tunnel tests that the most prominent BVI noise emission occurs when the blades azimuth angles are in the exactly range where the trailing vortices are nearly parallel to the blade.

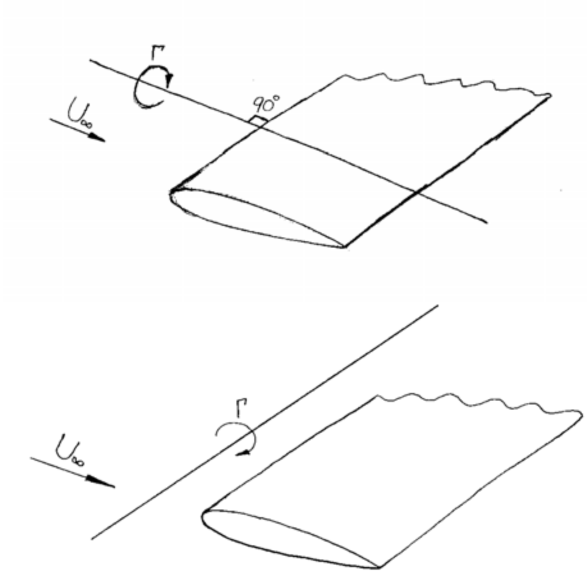

Figure 1: (a) Upper: vortex rotation axis perpendicular to the blade. (b) Lower: vortex rotation axis parallel to the blade.

In principle, the parallel BVI case sketched in Fig. 1b is easier studied because it can be approximated by a two-dimensional model. The entire span of the blade undergoes the same aerodynamic loading induced by the vortex filament. Strauss (Ref. 2) provides an excellent summary on the pioneering works performed on the problem of parallel BVI. In particular, in the work by Renzoni and Mayle (Ref. 3), a set of correlations was obtained for the overall change in the lift, moment and drag coefficients due to BVI. In this work, a formula for the maximum change in the lift coefficient is given in terms of the ratio between the normalized vortex circulation and the initial vertical distance between the vortex and the airfoil mean chord (the initial vortex-airfoil “mean distance”), which is considered a fundamental parameter to measure the intensity of the BVI phenomenon:

$$\Delta C_L = 0.7\frac{\Gamma/u_\infty c}{\sqrt{|y_0/c|}} = 0.7\frac{\overline{\Gamma}}{\sqrt{|y_0/c|}} \qquad (1)$$

In mathematical terms, the correlations as such imply that underlying kernels could be identified behind the phenomenon. The main objective of the present study is to demonstrate using the simpler two-dimensional formulation of parallel BVI that the Volterra integral series involving nonlinear kernels can identify the phenomenon. Moreover, in the present work a simple framework for the further developments of an engineering tool that can be used to obtain an accurate prediction of not only the overall change in aerodynamic coefficients during BVI but, most importantly, the associated time histories is established.

The pioneering work of the Italian mathematician Vito Volterra on functionals provided the fundamentals of modeling a physical process from some observable facts that can be used in turn to generate new information about the same process (Ref. 4). Due to the significant contributions by Wiener on the development of the Volterra functionals, this theory is also referred as the Volterra-Wiener theory of nonlinear systems. When modeling any nonlinear phenomena using the Volterra-Wiener theory, the effort is concentrated on the identification of the kernels associated with the series of integrals in either the time or the frequency domains. Although the initial identification of the kernels for a completely unknown process may be cumbersome, the advantages of using the Volterra integral series to generate reduced-order models outweigh these difficulties. This modeling technique allows the inclusion of any arbitrary number of degrees of freedom while maintaining simple levels of computations.

The Volterra-Wiener theory has long been used as a tool in the field of electrical engineering, mathematical biology, medical imaging and numerous other fields of applications. However, only in the past decade this powerful theory received attention from researchers in the field of unsteady aerodynamics. In 1990, Tromp and Jenkins (Ref. 5) applied for the first time a Volterra integral series identification scheme to model the nonlinear aerodynamics of a two-dimensional airfoil in subsonic flow subjected to an input angle of attack. The identification was performed in the frequency domain. The model was built using aerodynamic data produced by an unsteady Computational Fluid Dynamics (CFD) Navier-Stokes solver. Both the first-order (linear), and the second-order (non-linear) kernels were identified. Silva (Ref. 6) in 1993 also used the outputs from a CFD solver to identify the first and second-order kernels. His method, however, used the system responses to single- and double-impulse input functions to generate training datasets.

Reisenthel (Ref. 7) developed a method that identifies the Volterra kernels from unsteady aerodynamic training datasets obtained either from wind tunnel or flight tests. According to this method, in order to generate the training dataset the system is not required to undergo the experimentally difficult to reproduce impulsive excitations that are required in Silva's method. This is also an advantage when CFD-based datasets are used because impulsive inputs can only be approximated numerically. Reisenthel applied the method to a rigid NACA0015 airfoil that was dynamically pitched about its quarter chord. The results demonstrated that the method is feasible for the identification in the time-domain of the first and second-order Volterra kernels from experimental data. This method will be employed in the present work to identify BVI. First, a training dataset will be generated by a complete CFD analysis of the phenomenon, which includes assignment of the airfoil geometry, the flow field characteristics such as the Mach number, static temperature and pressure, and the single vortex specifications in terms of its circulation and core initial location with respect to the airfoil leading edge. If the vortex is released at a "sufficiently far" distance ahead the airfoil, only the vertical, y_0 coordinate, the vortex core initial miss distance becomes a parameter. Using the obtained training dataset, the Volterra kernels will be identified following Reisenthel's method. Once the reduced-order model is generated, the complete time-response of the system (regarded now as a "black box") will be predicted for a general input vortex, as depicted in Fig. 2. For this, the input vortex must be defined only in terms the time sequence given by the ratio between its normalized circulation and core instantaneous miss distance from the airfoil, $\alpha_{BVI}(t) = \bar{\Gamma}\big/\sqrt{|y(t)/c|}$. As (1) suggests, this ratio can be identified to an "equivalent instantaneous angle of attack" due to BVI that could also be directly related to the instantaneous lift coefficient, $C_L(t)$ experimented by the airfoil. This is, in summary, the object of study of the present paper: to identify a nonlinear model able to generalize Renzoni and Mayle's results for any time step. Although in the present work only the lift coefficient time history was the object of study, the time histories of other aerodynamic coefficients can be equally addressed using the same procedure, whose schematic is depicted in Fig. 3.

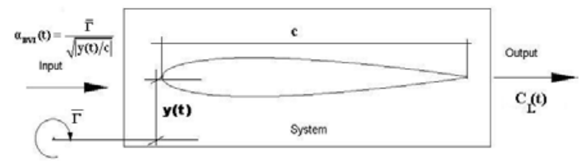

Figure 2: Unsteady aerodynamic system defined as a "black box"

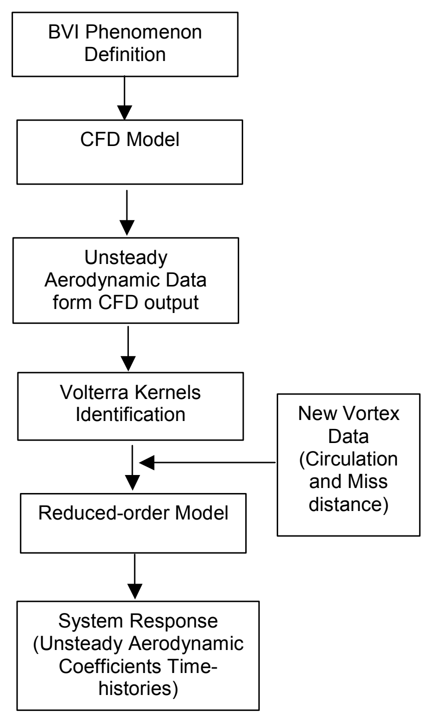

Figure 3: Reduced-order Model identification scheme

<u>Reduced-order Model Definition</u>

<u>Volterra Integral Series</u> The Volterra-Wiener theory states that any nonlinear system can be

modeled as an infinite sum of multi-dimensional convolution integrals (Ref. 8). Nonlinear systems exhibit an after-effect, which is often referred as the "nonlinear system memory." One example of such systems is BVI. The modeling of a nonlinear aerodynamic system with Volterra integrals follows a method of successive approximations. Starting from the conventional one-dimensional linear convolution, as many terms of an infinite series of multi-dimensional nonlinear convolutions containing kernels on time differences involving the present and previous instants of time are added as necessary to achieve an accurate description of the phenomenon.

The output of a nonlinear time-invariant system can be expressed by using the summation of the Volterra functionals as follows (Ref. 9):

$$z(t) = z_0 + z_1(t) + z_2(t) + z_3(t) + \dots \tag{2}$$

where z_0 is here a constant, $z_1(t)$ is known as the linear output, $z_2(t)$ is the bilinear output and $z_3(t)$ is the tri-linear output, etc. The order of each term in the series can be regarded as a measurement of the intrinsic non-linearity embedded into the system. For a weakly nonlinear system, only the first two Volterra functionals in the series are required to define the system, as the magnitudes of the higher-order kernels quickly fall off, and these terms become negligible.

The Volterra functionals in (2) are given by:

$$\begin{aligned} z_1(t) &= \int_0^t K_1(t-\tau_1)\alpha(\tau_1)d\tau_1 \\ z_2(t) &= \int_0^t\int_0^t K_2(t-\tau_1,t-\tau_2)\alpha(\tau_1)\alpha(\tau_2)d\tau_1 d\tau_2 \\ z_3(t) &= \int_0^t\int_0^t\int_0^t\big[K_3(t-\tau_1,t-\tau_2,t-\tau_3) \\ &\qquad \alpha(\tau_1)\alpha(\tau_2)\alpha(\tau_3)d\tau_1 d\tau_2 d\tau_3\big] \end{aligned} \tag{3}$$

where t is the current instant of time, τ_1, τ_2 and τ_3 are dummy time integration variables; $\alpha(t)$ is the system input, K_1, K_2 and K_3 are the kernels of the Volterra series, and $z(t)$ is the overall system response to the input function, $\alpha(t)$.

The prediction of the nonlinear aerodynamic response of a system to an arbitrary input begins from the identification of the kernels of the Volterra integrals. The procedure is essentially the same regardless the order of the kernel. The system response due to an arbitrary input can be obtained either from experimental datasets or from the output of a CFD simulation, as it was done in the present work. The extraction of the kernels is the most critical part of the prediction process because they hold the characteristics of the physical system. The first task in the extraction process involves discretization of the unknown kernels in the time domain and their subsequent expansion into a space spanned by prescribed basis functions:

$$\begin{aligned} K_1(t) &= \sum_j c_j \zeta_j(t) \\ K_2(t_1,t_2) &= \sum_k d_k \mu_k(t_1,t_2) \end{aligned} \tag{4}$$

In (4), the basis functions ζ_j and μ_k are admissible functions of time, whereas c_j and d_k are coefficients to be determined. These must satisfy all available datasets at all times in a least-square sense. Since the solution of this least square problem is highly sensitive to round off errors, a singular value decomposition technique is employed (Ref. 7).

Thus, for the i^{th} time step the bilinear representation of the nonlinear system in terms of the prescribed basis functions gives:

$$\begin{aligned} z(t_i) &= \sum_j c_j \int_0^{t_i}\zeta_j(t_i-\tau_1)\alpha(\tau_1)d\tau_1 + \\ &\sum_k d_k \int_0^{t_i}\int_0^{t_i}\mu_k(t_i-\tau_1,t_i-\tau_2)\alpha(\tau_1)\alpha(\tau_2)d\tau_1 d\tau_2 \end{aligned} \tag{5}$$

<u>Tailoring Kernel Basis Functions for BVI.</u> In the present work, it was found that the lift response of the airfoil due to BVI could not be modeled with the bilinear approximation using the basis functions discussed in Ref. 7. Due to the highly nonlinear characteristics of the phenomenon, a higher-order model containing several additional Volterra functionals would be necessary. This would make the process of kernel identification of Ref. 7 too cumbersome and not well suited to the envisioned development a simple engineering tool to predict BVI. Roughly, the lift curves due to BVI resemble two consecutive delta functions carrying opposite signs (or the derivative of a delta function). Then, in the present work it is proposed that the form of the second-order basis functions of Ref. 7, which define the bilinear kernel be modified to tailor the present application. To better describe the impulsive BVI phenomenon, an extra term

resembling the Gauss probability function was added to the original set of basis functions μ_k associated with the bilinear kernel, whereas the basis functions ζ_j associated with the linear kernel remained unchanged. Therefore, the first and second-order basis functions depicted in (5) in the present work are given by, respectively:

$$\zeta_j(t) = e^{-\frac{t}{\tau_j}}$$
$$\mu_k(t_1,t_2) = e^{-\left(\frac{t_1}{\tau_{1k}}+\frac{t_2}{\tau_{2k}}\right)} + e^{-\left(\frac{t_2}{\tau_{1k}}+\frac{t_1}{\tau_{2k}}\right)} + \underline{\frac{1}{\sqrt{\pi}} e^{-\frac{t_2^2}{\tau_{2k}^2}}} \qquad (6)$$

where the underlined term in the second expression is the proposed addition. Also in (6), τ_{1k} and τ_{2k} are time constants that are determined at this stage of development of the method by a procedure that is greatly dependent upon past experience and "educated guesses." Fundamentally, the range of values of the time constants are chosen to cover a range bounded by the inverse of the time interval defined by the signal onset (i.e., when the lift produced by the approaching vortex is first detected) and the time at which the final value of the input is reached (i.e., when the maximum lift due to the approaching vortex is reached). Therefore, by adjusting the time scales, the frequency content of the input signal is controlled. The impact of choosing the correct time scales is important to improve the efficiency and accuracy of the method. Hence, the time scales must be tested in an algebraic sequence to determine their proper values. For the first-order basis functions, ζ_j the trial set of time constants, τ_j are kept in a one-dimensional array. Once these values are selected, they are left unchanged while identifying the second-order kernel. The basis functions for the second-order kernel, μ_k are constructed to span a similar range of time scales covered by the first-order kernel. In this case, the time constants, τ_{jk} are the elements of a symmetric matrix formed by all possible combinations from the generating set. For example, for a generating set of consisting of three time constants, forming the array [τ_1, τ_2, τ_3], nine second-order time-constants are obtained as follows:

$$\left[\tau_{jk}\right] = \begin{bmatrix} \tau_{11} & \tau_{12} & \tau_{13} \\ \tau_{21} & \tau_{22} & \tau_{23} \\ \tau_{31} & \tau_{32} & \tau_{33} \end{bmatrix} \equiv \begin{bmatrix} \tau_1 & \tau_2 & \tau_3 \\ \tau_2 & \tau_3 & \tau_1 \\ \tau_3 & \tau_1 & \tau_2 \end{bmatrix} \qquad (7)$$

Importantly, by imposing the above symmetry on the second-order time constants matrix, one guarantees a fundamental symmetry property of the kernel. It is, however, important to note that when adding the underlined term in (6), the space spanned by the basis functions is no longer complete and this fact should raise mathematical concerns that must be addressed in the future.

Forming the BVI Dataset

CFD Simulation Model. In the present study, the blade-vortex interaction was first modelled numerically by solving Euler/Navier-Stokes equations using a finite-volume commercial solver. Since the purpose of the simulations was only to create a nonlinear dataset for the Volterra kernel identification process, the simpler Euler-based option of the CFD solver was employed. When choosing the Euler model, the flow is assumed inviscid, and the BVI cannot cause flow separations. Hence, in all simulations the vortex was initialized at a miss distance below the airfoil where the resulting vortex path did not lead to a direct head-on collision with the airfoil, ensuring that the above assumptions were valid.

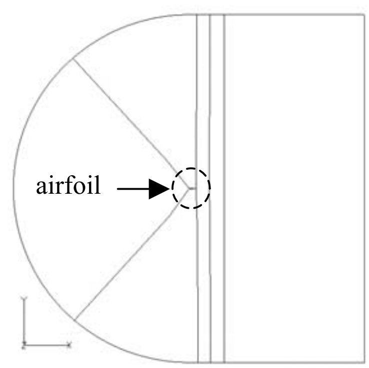

Figure 4: Domain outlines for the NACA 0012 airfoil mesh.

The accuracy of the simulation results is strongly dependent on the details of the blade geometry and the mesh. The geometry used in the simulation was the symmetric NACA 0012 airfoil with a unit chord length. The airfoil was set at a position with a 0^o angle of attack; therefore, any lift observed in the simulations was a direct result from the blade-vortex interaction. A C-type, multi-zone two-dimensional structured grid was constructed around the airfoil. The outer boundaries were located 25 chords away from the nose of the airfoil. The computational domain was divided into 6 zones, as shown in Fig. 4, allowing different grid densities to be used in different areas around the airfoil. During the simulation of BVI, a very fine grid was required on the path of the vortex in order to preserve its characteristics. Throughout the study, the vortex was set so that it passed under the target airfoil; therefore the zones directly in front of and under the airfoil contain the highest grid density. The grid was constructed in such a way that the near field of the airfoil contained a very fine grid distribution that gradually coarsened as it proceeded outward towards the far field. The total number of grid points was approximately half-a-million. The same grid was used for all of the computations. Using the same grid topology with a larger value for the normal distance resulted in fewer grid points but the dissipation of the minimum pressure inside the core was found to be too great; therefore, the fine grid was selected for the present analysis.

At the solid boundaries (the upper and lower surfaces of the airfoil) inviscid (slip) and adiabatic wall conditions were applied. The normal pressure gradient at the wall was assumed to be zero. The ideal gas model was used in the simulations. The freestream flow field conditions were used as reference conditions for normalizing the flow field variables (Table 1). At the downstream (outflow boundary), the pressure for all the points on the boundary was extrapolated from the adjacent points.

Mach Number	0.300
Speed of Sound	1116 ft/s
Flow Velocity	334.9 ft/s
Total pressure	15.643 psia
Static pressure	14.696 psia
Total temperature	528.0°R
Static temperature	518.7°R

Table 1: Flow-field characteristics

A single vortex with the non-dimensional circulation $\overline{\Gamma} = \Gamma / u_\infty c = 0.166$ in the clockwise direction was released downstream at the fixed freestream velocity, u_∞ in all test cases. Since for a typical rotor blade the tip vortex has a core diameter of about the thickness of the blade (Ref. 10), the radius was set as 6% of the chord length to match the NACA 0012 airfoil used in the simulations. The internal structure of the vortex was constructed according to the classical vortex model suggested by Scully (Ref. 11). The leading edge of the airfoil was positioned at the origin of the Cartesian system, (x, y). For each of the simulations, the vortex was initially placed at a horizontal distance of approximately x_0=2.5 chords ahead of the airfoil (considered "far enough") and different vertical miss distances, y_0 below the airfoil. The vertical distance was measured in all cases from the chord line of the airfoil to the core of the vortex. The definition of the CFD problem initial conditions is summarized in Fig. 5.

An array of test cases with different miss distances was simulated in the present study. The exact initial locations, (x_0, y_0) of the core for test cases studied are listed in Table 2. This set of test cases was selected to cover a narrow range of miss distances so that the extraction of kernels could be performed within a minimum number of test cases. A fifth-order upwind-biased spatial integration scheme was used and the time step was set at 2.5μs, with 20 maximum iteration cycles per time step.

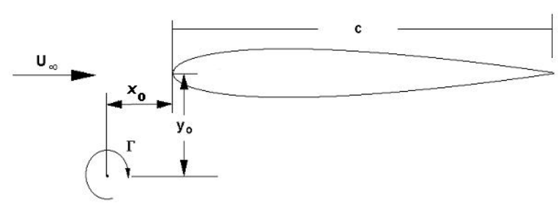

Figure 5: Definition of Test Cases initial conditions.

Test Case Number	x_0/c	y_0/c
1	~2.53480	~0.245929
2	~2.54205	~0.155371
3	~2.52202	~0.353106
4	~2.53898	~0.19865
5	~2.52461	~0.334044
6	~2.53028	~0.288505
7	~2.54062	~0.176521
8	~2.54161	~0.162314
9	~2.54012	~0.183789

Table 2: Initial location of the vortex core for Test Cases.

<u>CFD Simulation Results.</u> Since the only notable difference among all test cases was the initial

miss distance, y_0 the description of the airfoil-vortex interaction process is discussed for one of the test cases in the present work. The instantaneous pressure coefficient contours in Figs. 6 to 11, along with the airfoil lift coefficient time history in Fig. 8 will now be examined for Test Case 9.

Beginning with Fig. 6, the vortex is located at 0.485 chords ahead of the airfoil. At this location the vortex starts to interact with the airfoil, as the pressure coefficient contour indicates.

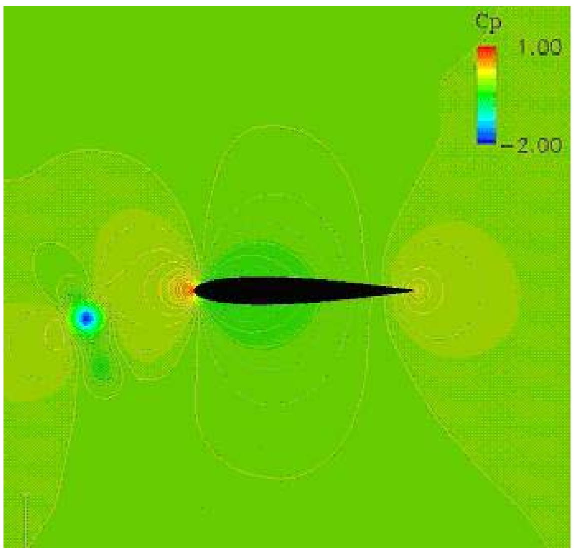

Figure 6: Pressure coefficient contour of Test Case 9 at 0.00705s (BVI starts).

In Fig. 7, the vortex has advanced towards the leading edge of the airfoil. The approach of the clockwise rotating low-pressure vortex causes the lower surface of the leading edge of the airfoil to become a low-pressure region. When the vortex is located at 0.00848 chords and the core of the vortex has just passed the nose of the airfoil, the minimum pressure coefficient over the airfoil peaks to a high of approximately 1.0. As a result of this rapid decrease in pressure over the lower surface, the lift coefficient over the airfoil also experienced a plunge from zero to −0.15, as shown in Fig. 8. Also from Fig. 8, once the vortex passes the nose of the airfoil, the lift induced by the vortex rapidly increases and reaches its maximum value of 0.047. This rapid increase in lift is associated with the magnitude of the negative pressure peak induced by the vortex on the lower surface of the airfoil.

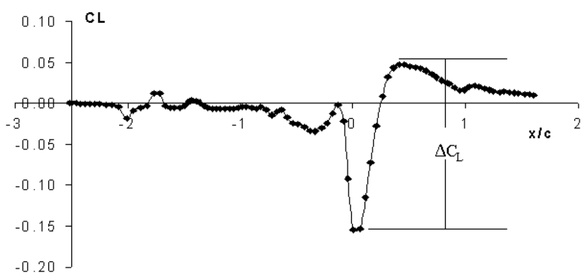

Figure 8: Airfoil instantaneous lift-coefficient versus vortex positions for Test Case 9.

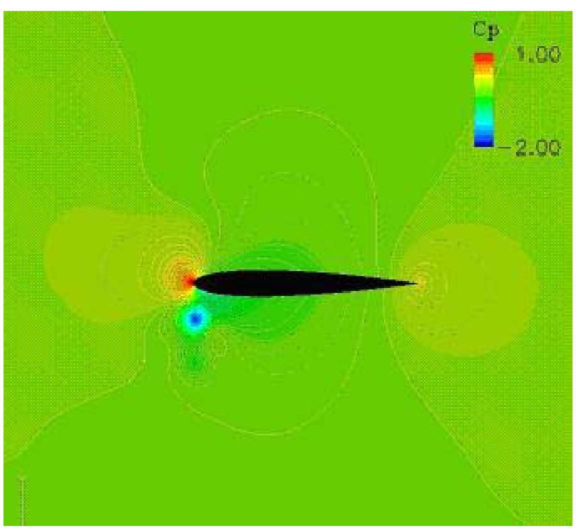

Figure 7: Pressure coefficient contour of Test Case 9 at 0.00855s (BVI peaks).

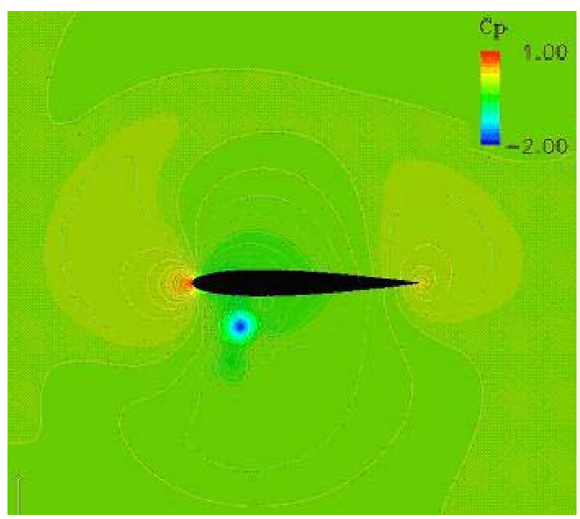

Figure 9: Pressure coefficient contour of Test Case 9 at 0.00915s.

It can be seen in subsequent time sequences (Figs. 9 to 11) that the propagation of the pressure peak towards the trailing edge corresponds to the convection of the vortex. As the negative pressure coefficient peak decreases, the overall pressure on the lower surface of the airfoil also becomes less negative. Hence, the normal velocity induced by the vortex has the effect of increasing the airfoil effective angle of attack. The lower surface becomes a higher-pressure region and, therefore, the lift increases in the process. In the pictures, it can also be seen a slight and noticeable decrease in the vortex intensity due to the numerical dissipation inherent to the CFD approach. However, since the focus of the present study is on the development a reduced-order model based on a typical case of parallel BVI, these results were considered satisfactory.

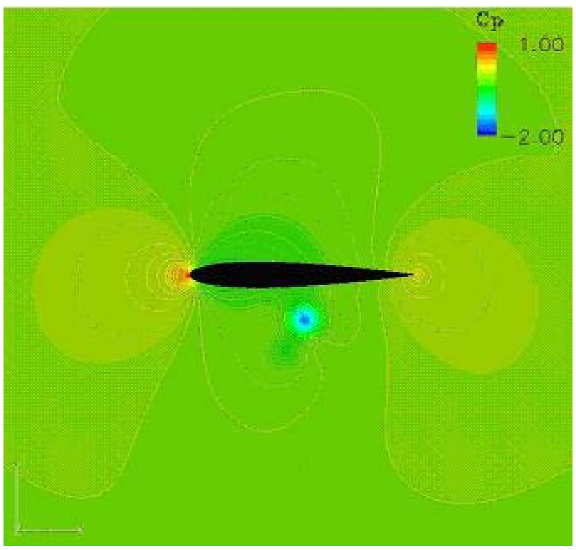

Figure 10: Pressure coefficient contour of Test Case 9 at 0.01005s.

Figure 12 depicts the situation when the vortex reaches the trailing edge of the airfoil (the core is located at 1.03 chords). With the negative pressure coefficient peak located at the trailing edge, the airfoil experiences a small increase in lift. This small increase in lift translates into the small bump in the lift coefficient time-history shown in Fig. 8. Even after the vortex has passed the airfoil, its effect continues to linger until it is a few chords downstream, as the same picture indicates. Also, as Fig. 12 suggests, the numerical dissipation problem becomes more evident at this stage. Hence, the present CFD results underestimate the lingering effects of BVI.

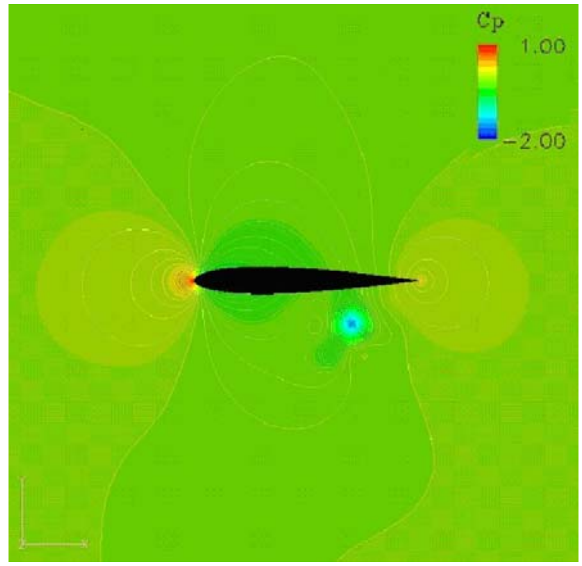

Figure 11: Pressure coefficient contour of Test Case 9 at 0.01065s.

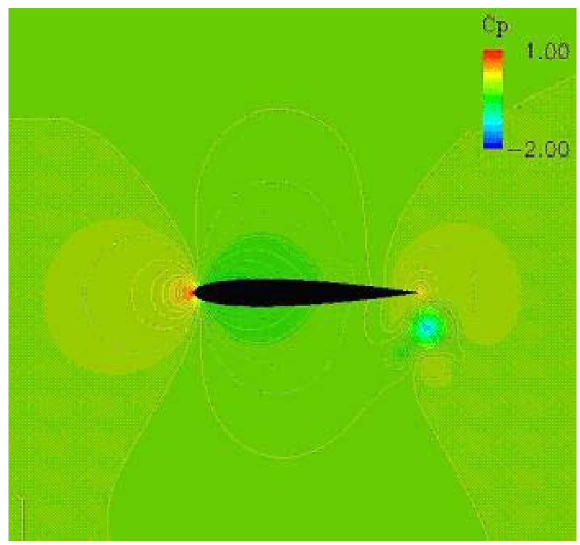

Figure 12: Pressure coefficient contour at 0.01185s (vortex at trailing edge).

A summary of the lift coefficient time histories for all Test Cases studied is shown in Fig. 13. In Fig. 14, the corresponding normalized maximum change in the lift coefficient for all test cases is plotted against the predictions of Renzoni and Mayle (Ref. 3). According to the same Figure, the present CFD simulations correlated fairly well with the formula in (1). The deviations are probably due to poorer convergence of the CFD code in some test cases, indicating that the set allowed maximum of 20 iteration cycles should be increased to guarantee convergence for all test cases.

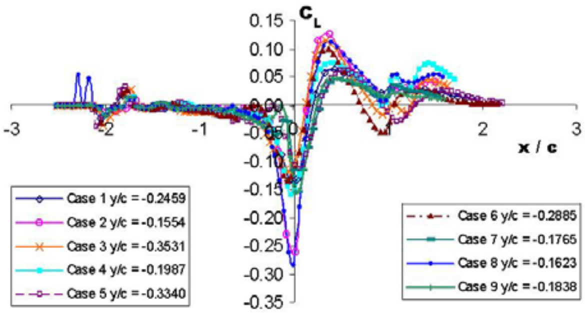

Figure 13: Airfoil lift-coefficient versus vortex instantaneous position for Test Cases 1 to 9.

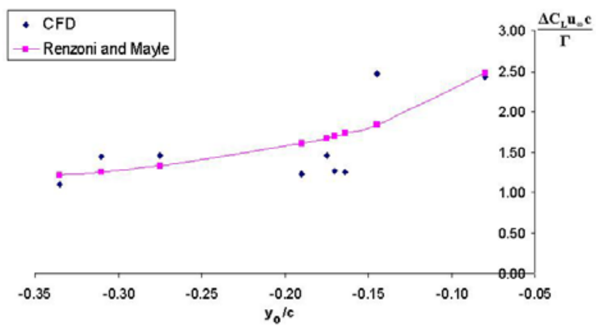

Figure 14: Comparison of airfoil maximum change in lift-coefficient versus vortex core initial miss distance against Renzoni and Mayle's predictions (Ref. 3) for Test Cases 1 to 9.

Volterra Kernels Identification

For the Volterra kernels identification process, Test Cases 3 to 9 were used. Test Cases 1 and 2 were left out of the process so that they could be used as new data for validation of the method. The training dataset spanned by these seven test cases covered a range of normalized vortex initial miss distances, y_0/c from –0.145 to –0.335.

As commented in a previous Section, the selection of the time constants to represent the admissible basis functions is critical to the kernel identification process. At the beginning of the kernel identification process, a range of time scales has to be tested in an algebraic sequence in order to determine their proper values. At first, as nothing was known about the system, several series of positive time constants sets were used in the testing. The first-order kernel was chosen to have six time constants that were kept constant throughout the process: [0.3, 0.2402, 0.1804, 0.0907, 0.0309, 0.001]. The identification of the second-order kernel proved to be more difficult due to the highly nonlinear characteristics of the phenomenon. Due to the chosen form for the basis functions, only positive constants provide stability to the model. After conducting a series of tests, it was found that a bilinear-based reduced-order model formed with only exponentially decreasing basis functions (bearing positive time constants) could not capture the rapid changes in the lift time-history, as shown in Fig. 15. In this Figure, the second-order kernel was based on the 6x6 symmetric matrix of time constants formed with the array [1.5, 1.35, 1.05, 0.75, 0.45, 0.005].

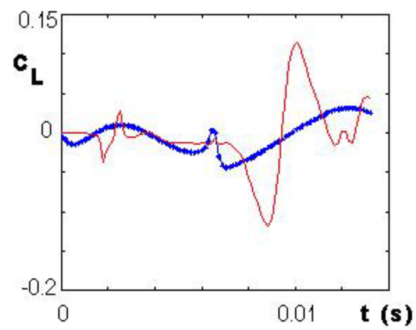

Figure 15: Lift coefficient versus time for Test Case 3. Comparison of bilinear model based on the conventional basis functions (blue curve) against CFD simulation (red curve).

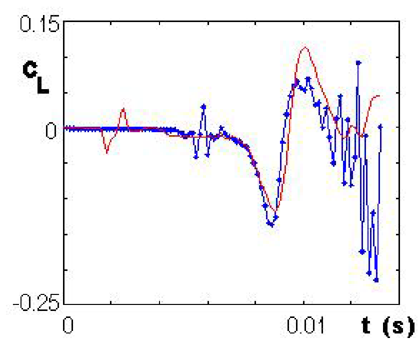

Figure 16: Lift coefficient versus time for Test Case 3. Comparison of bilinear model based on the conventional basis functions and some increasing exponentials (blue curve) against CFD simulation (red curve).

Still retaining the bilinear approximation, a better capture of the BVI transient was found using for the second-order kernel a number of higher-frequency content exponentially increasing basis functions. The agreement with the simulation data showed significant improvement, as shown in Fig. 16. However, as expected, instability builds up rapidly after the maximum lift is achieved. In this example, the second-order kernel was based on the 8x8 symmetric matrix of time constants formed with the array [0.1, 0.01, 0.005, –0.0015, –0.0018, –0.0022, –0.0025, –0.003]. Nevertheless, a much-improved agreement with the dataset could be obtained by adding the underlined term to the basis functions defining the second-order kernel, as indicated in the second of Equation (6). The results are depicted in Fig. 17. In this example, although the array of time constants from the previous example was kept, the instability was offset. Moreover, inspection of Figs. 15, 16 and 17 prove that the modified second-order kernel brought a significant improvement into the bilinear model approximation. The lingering oscillations shown in Fig. 16 are no longer persistent in Fig. 17. Although the extremes of the lift response were not well captured in Fig. 17, the bilinear model replicated the general characteristics of the CFD simulations.

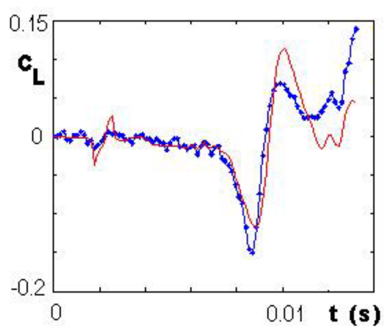

Figure 17: Lift coefficient versus time for Test Case 3. Comparison of bilinear model based on the modified basis functions (blue curve) against CFD simulation (red curve).

Reduced-order Model Predictions

Once the kernels were identified, the system is replaced by a "black box" and its response due to a new input (to which it has never been exposed during the identification process) can be predicted. In the upcoming predictions, it is worthwhile to stress that the input of the system is given by the time sequence corresponding to the instantaneous angle of attack due to BVI, previously defined in Fig. 2, and given by the ratio between the normalized vortex circulation and the core instantaneous normalized vertical position (miss distance) from the airfoil, $\alpha_{BVI}(t) = \bar{\Gamma} \big/ \sqrt{|y(t)/c|}$. The considered output of the system is the lift time history, $C_L(t)$.

Test Cases 1 and 2, which were not used in the kernels identification process, represent new data to demonstrate the performance of the reduced-order model. Test Case 1 is well within the y_0/c range covered by the training dataset, while Test Case 2 is outside, consisting thereof a more difficult case. The output lift responses predicted by the method are shown in Fig. 18 and Fig. 19, respectively, for Test Case 1 and Test Case 2.

The predicted lift response shown in Fig. 18 compared very well with the numerical simulation solution. Even though the minimum was slightly over predicted, the maximum was in very good agreement with the CFD simulation. As for the more severe case of the two, Test Case 2, although the minimum and maximum were not very well captured, as Fig. 18 indicates, the predicted lift response did present the general characteristics of the CFD simulation.

It is important to stress the fact the accuracy of the extracted Volterra kernels could be significantly improved by using datasets with a larger number of test cases and covering a wider range of airfoil-vortex miss distances. In fact, the number of nine CFD Test Cases included in the dataset employed in the kernels identification process is very limited when compared with its counterpart presented in Ref. 7.

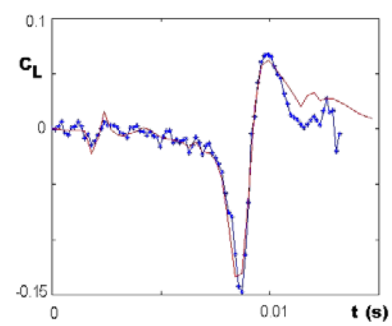

Figure 18: Lift coefficient versus time for Test Case 1 (predicted by the model). Comparison of bilinear model based on the modified basis functions (blue curve) against CFD simulation (red curve).

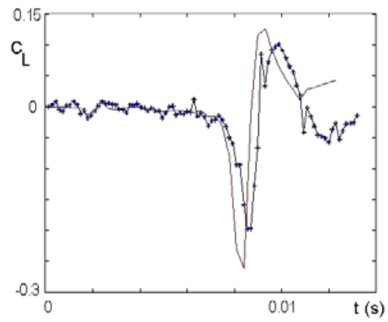

Figure 19: Lift coefficient versus time for Test Case 2 (predicted by the model). Comparison of bilinear model based on the modified basis functions (blue curve) against CFD simulation (red curve).

Conclusions:

The theory of Volterra-Wiener for nonlinear systems identification was applied to predict the lift time history of an NACA 0012 airfoil subjected to typical parallel blade-vortex interaction (BVI) phenomenon. The airfoil and its surrounding flow field composed the "black box" nonlinear system to be identified. The time sequence defined by the instantaneous vortex core miss distance with respect to the airfoil mid chord was considered the system input, whereas the lift coefficient time history was regarded the output. First, aerodynamic data obtained from CFD simulations was used to build a training dataset for the "black box." A reduced-order model of the system based on the Volterra series bilinear approximation, retaining only its linear and first nonlinear functionals, was next generated. The reduced-order model was then exposed to input data not included in the training dataset. The prediction results were shown to be in fairly good agreement with the corresponding CFD simulations, suggesting that the outlined method is promising.

References:

[1] Martin, R. M. and Splettstoesser, W. R., "Blade-Vortex Interaction Acoustic Results from a 40% Model Rotor in the DNW," *American Helicopter Society J.*, Vol. 33, No. 1, 1988.

[2] Strauss, J., *Pressure and Velocity Measurements About An Airfoil During a Parallel Blade-Vortex Interaction*, Ph.D. Thesis, Rensselaer Polytechnic Institute, NY, 1991.

[3] Renzoni P. and Mayle, R. E., "Incremental Force and Moment Coefficients for a Parallel Blade-Vortex Interaction," *AIAA J.*, Vol. 29, No. 1, 1991.

[4] Burton, T. A., *Volterra Integral and Differential Equations*, Academic Press, Inc., NY, 1983.

[5] Tromp, J. C. and Jenkins, J. E.,"A Volterra Kernel Identification Scheme Applied to Aerodynamic Reactions," *AIAA Paper* No. 90-2803, 1990.

[6] Silva, W. A., "Application of Nonlinear Systems Theory to Transonic Unsteady Aerodynamic Responses," *J. of Aircraft*, Vol. 30, No. 5, 1993.

[7] Reisenthel, P. H., *A Nonlinear Volterra Kernel Identification System for Aeroelastic Applications*, Report NEAR TR-547, Nielsen Engineering & Research, Inc., Mountain View, CA, June 1999.

[8] Cochran, J. A., *The Analysis of Linear Integral Equations,* Bell Telephone Labs, Inc., NY, 1972.

[9] Bendat, J. S., *Nonlinear System Analysis and Identification From Random Data*, John Wiley & Sons, Inc., NY, 1990.

[10] Srinivasan, G. R., McCroskey, W. J., and Baeder, J. D., "Aerodynamics of Two-dimensional Blade-Vortex Interaction, "*AIAA J.*, Vol. 24, No. 10, 1986.

[11] Johnson, W., *Helicopter Theory*, Dover Publications, Inc., NY, 1980.